In Situ Analysis

DOI: 10.1002/anie.201008214

Determination of Molecular Surface Structure, Composition, and Dynamics under Reaction Conditions at High Pressures and at the Solid–Liquid Interface**

Gabor A. Somorjai, Simon K. Beaumont, and Selim Alayoglu*

heterogeneous catalysis · in situ studies · interfaces · nanoparticles · surface analysis

Dedicated to the Fritz Haber Institute, Berlin, on the occasion of its 100th anniversary

In the last two decades, surface-science experiments and techniques have been developed to focus on obtaining molecular information under reaction conditions at high pressures (near or above 1 bar) and liquid interfaces. This Minireview describes the results of these studies obtained by surface-sensitive laser spectroscopies, scanning tunneling microscopy, and X-ray spectroscopies usually practiced at a synchrotron light source. The use of model surfaces, single crystals, and monodisperse nanoparticles with variable size (1–10 nm) and shape facilitates meaningful interpretation of the experimental data. These methods allow evaluation of the molecular structures of intermediates, oxidation states of metals, and mobility of adsorbants. New techniques that are likely to make major contributions to the investigation of surfaces under reaction conditions are also discussed.

1. Introduction

Catalysis is one of nature's most pervasive chemical phenomena. It is usually divided into three branches that reflect the conditions in which they appear to predominantly operate: heterogeneous, homogeneous, and enzyme at both gaseous–solid and liquid–solid interfaces and in a certain temperature range of optimum utility for major applications. Traditionally the catalysts were characterized before and after the reaction studies with the available techniques, but they could not be characterized during the reaction, because techniques that provide atomic- and molecular-scale information under reaction conditions were not available. Although pre- and postcatalysis characterization may provide useful glimpses of what is happening under reaction conditions,[1] in order to remedy this state of affairs catalysis research embarked on investigations in two directions, which show a certain synergism: 1) development of techniques that are sensitive to the buried interfaces (solid–gas and solid–liquid) and provide molecular information and 2) use of model catalysts which provide the uniformity of structure to permit structure–function correlations with relative ease once the instruments have provided the experimental data under the reaction conditions. This second point concerning the development and use of model catalysts (at odds with many attempts to do so using complex and poorly defined non-model systems) is crucial for reducing the number of variables to allow any understanding of catalytic chemistry at a molecular level (something explored in more detail elsewhere).[2] However it is the development and need for instrumentation working under reaction conditions that is the focus of this Minireview. Using these new techniques and model catalysts in recent years, we identified seven key molecular factors that control catalytic selectivity.[3]

Herein we focus on a number examples showing how these key factors vary dramatically when studied under reaction conditions, in particular focusing on examples obtained using instruments that we currently use most frequently in our laboratory for this purpose. These are 1) sum-frequency-generation (SFG) vibrational spectroscopy

[*] Prof. G. A. Somorjai, S. K. Beaumont, S. Alayoglu
Department of Chemistry, University of California
Berkeley, CA 94720 (USA)
and
Materials Science Division, Lawrence Berkeley National Laboratory
Berkeley, CA 94720 (USA)
E-mail: somorjai@berkeley.edu

[**] This work was supported by the Director, Office of Energy Research, Office of Basic Energy Sciences of the U. S. Department of Energy under Contract DE-AC02-05CH11231.

and 2) high-pressure scanning tunneling microscopy (HPSTM), which can be accomplished in the laboratory, along with three further techniques, each making use of the Advanced Light Source (ALS) synchrotron (Berkeley, CA, USA): 3) ambient-pressure X-ray photoelectron spectroscopy (APXPS), 4) total-electron-yield near-edge X-ray absorption fine structure (NEXAFS) spectroscopy and 5) extended X-ray absorption fine structure (EXAFS) spectroscopy. Each of these techniques has been found to provide vital insights into the workings on the molecular level of many catalytic systems (both from our laboratory and elsewhere), which would not have been obtained without studying them during the reactions—in many examples the changes occur reversibly when the system is cycled between reactive and nonreactive environments (by changing the pressure, gas composition, or another reaction parameter).

2. Sum-Frequency-Generation (SFG) Vibrational Spectroscopy

This method, first developed by Shen and co-workers in 1986,[4,5] is arguably the surface-science technique that from its infancy has lent itself to application in high-pressure studies, owing to its absolute sensitivity to interfacial phenomena, irrespective of the medium in which the interface may be buried. SFG is a nonlinear optical process and is caused by higher-order perturbations in the electrostatic polarization of light. In its most useful form, these second-order nonlinear optical interactions cancel to zero in centrosymmetric media (gases, liquids, and amorphous solids), while for non-centrosymmetric media, such as crystal surfaces and all interfaces, they become comparable in amplitude, and so a signal is observed. This signal response to the feature of interest is a linear term and therefore can be used quantitatively. This quantitative relationship can then be exploited to study surface-catalyzed processes by indentifying adsorbed surface species.

In simple terms, the SFG signal is generated from two or more input optical waves (usually lasers) which overlap in time and space at the sample (Figure 1). Typically these comprise a fixed-frequency (static) visible component and a second component in the infrared regime that can be tuned in frequency. It is this ability to tune the frequency of one of the input waves—and therefore the energy of chemical bonds that can be excited—that allows exploitation of this phenomenon for vibrational spectroscopy, whether for adsorbate molecules on crystal surfaces or on metal nanoparticle films or for organic and bioorganic molecules at solid–liquid interfaces.

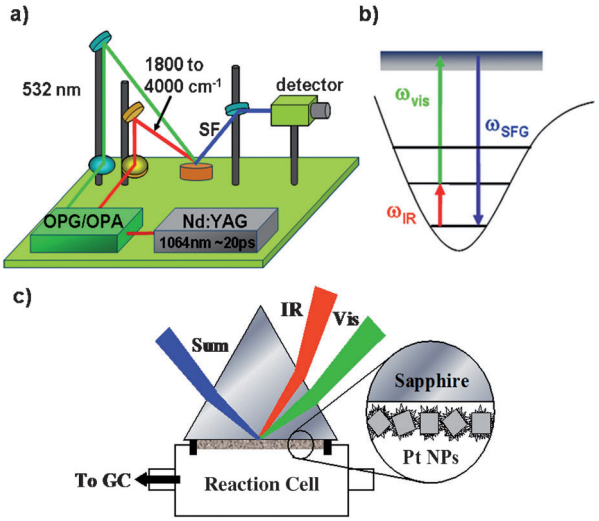

Figure 1. Sum-frequency-generation vibrational spectroscopy: a) a typical experimental setup in which lasers of two frequencies are combined spatially at the sample to produce a 'sum-frequency' signal that is then detected; b) the different energies of the incident photons can combine to give the sum-frequency-energy photons as a result of molecular bond vibrations in an adsorbate; c) a typical reaction cell used in our laboratory to study reactions at supported nanoparticles in real time using this technique and also incorporating online gas chromatographic analysis. OPG/OPA = optical parametric generation/optical parametric amplification, SF = sum frequency, NPs = nanoparticles, YAG = yttrium aluminum garnet.

SFG has been utilized for the study of surfaces for only a few decades, yet it has contributed to the understanding of a number of surface-related phenomena on a truly molecular basis. In particular, two quite different case studies from our research group provide insight into the development of fundamental molecular-based surface chemistry using this technique. Firstly, reactions of ethylene, cyclohexene, and benzene with H_2 on platinum single-crystal or nanoparticle surfaces and, secondly, the interaction of amino acids with hydrophobic polymer and hydrophilic silica surfaces.

Ethylene hydrogenation is a model case for illustrating the high-pressure surface-specific capabilities of SFG vibrational spectroscopy. Ethylene hydrogenation on Pt surfaces is exothermic and is known to involve three reaction species: ethylidyne, σ-bonded ethylene, and π-bonded ethylene. Catalytic studies suggested the nature and mechanism of this reaction, but no direct molecular evidence had ever been presented. From prior catalytic studies and ultrahigh-vacuum (UHV) experiments, it was anticipated that the ethylidyne species is a spectator, while π-bonded ethylene is the active adsorbate geometry and leads to an ethyl intermediate. Spectroscopic techniques other than SFG vibrational spectroscopy are usually restricted to the study of surfaces in vacuum, where overlapping signals from the gas-phase

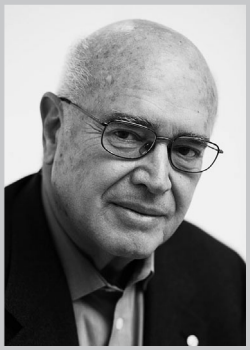

Gabor A. Somorjai is Professor of Chemistry at the University of California, Berkeley and Senior Faculty Scientist at the Lawrence Berkeley National Laboratory, where he has educated more than 130 Ph.D. students and about 250 postdoctoral fellows. Professor Somorjai has received nearly every award in his field, among them the 2010 BBVA Foundation Frontiers of Knowledge Award, the Priestley Medal (2008), the National Medal of Science (2002), and the Wolf Prize (1998). He is the author of more than 1100 scientific papers and three text books.

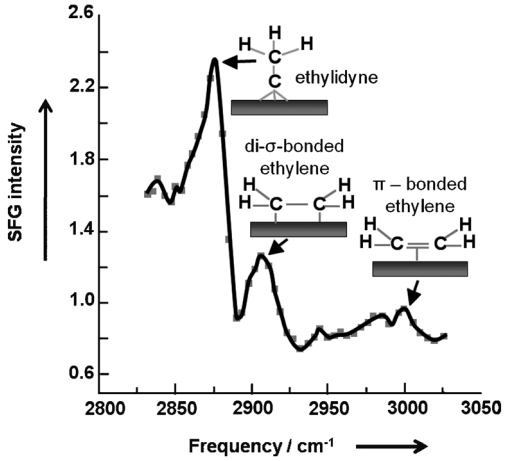

Figure 2. SFG spectrum of the Pt(111) surface during ethylene hydrogenation with 100 Torr H_2, 35 Torr C_2H_4, and 615 Torr He at 295 K highlighting the three key surface species.

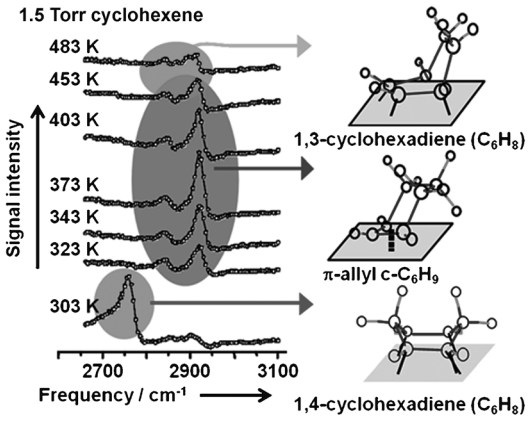

Figure 3. Temperature-dependent SFG spectra of surface species on Pt(111) under 1.5 Torr cyclohexene in the range 303–483 K. The key surface species in each temperature region is indicated.[7]

molecules do not obscure the surface-derived spectral features. By using infrared–visible SFG spectroscopy with simultaneous gas-chromatographic kinetic studies (Figure 2), we can see all three relevant species on the surface under reaction conditions (1 atm H_2/ethylene/He mixture). This result demonstrated that ethylidyne and σ-bonded ethylene species are indeed spectators and do not contribute to catalytic turnover, while the turnover rate associated with π-bonded ethylene present on the catalyst surface is several orders of magnitude higher, despite its surface concentration being only about 0.04 monolayers (ML). SFG also allowed the first observation of the ethyl intermediate in this reaction, thus confirming the role of all species present in the mechanism of ethylene hydrogenation.[6]

In addition to helping elucidate the mechanism of a reaction, spectroscopic interrogation under reaction conditions can also lead to an understanding of selectivity, which is a crucial figure of merit for any catalytic process. This is true for the platinum-catalyzed reaction of cyclohexene with hydrogen—a model reaction that can either result in hydrogenation to cyclohexane at relatively low temperatures or mostly dehydrogenation to benzene at higher temperatures (above 480 K). SFG spectroscopy has allowed determination of the active surface species even under conditions where both reactions occur concurrently by studying Pt(111) surfaces under various pressures of cyclohexene and hydrogen. Significantly, the cyclohexyl π-allyl c-C_6H_9 species (c = cyclic), which is the active intermediate in UHV at room temperature, is not detected at ambient pressures.[7] However, SFG vibrational spectra reveal the presence of all three intermediate surface species as the temperature is varied (Figure 3): 1,4- and 1,3-cyclohexadiene as well as π-allyl c-C_6C_9.

Unlike ethylene hydrogenation, the cyclohexene hydrogen reaction is known to be structure-sensitive: the rates, reaction pathways, and intermediates depend strongly on the nature of the metal surface. SFG spectroscopy allowed identification of different surface intermediates present on Pt(100) and Pt(111) under reaction conditions and, thus, in combination with kinetic data and energetic calculations, led to a molecular-level understanding of the different mechanisms behind this structure sensitivity.[8]

In the introduction, the importance of using model systems was highlighted. While offering a way of understanding the molecular mechanics of a reaction, the applicability of simple models to "real life" is often questioned; accordingly, it is advantageous to produce progressively more realistic model materials, and use of supported size- or shape-controlled nanoparticles is an attractive strategy for achieving this goal. SFG spectroscopy can be deployed in the case of reactions occurring on both single-crystal and supported-nanoparticle surfaces and is therefore worth noting as also being a valuable tool in evaluating whether our understanding can bridge this "materials gap" effectively. To this end, shape-controlled Pt NPs with cube and cuboctahedra morphologies have been synthesized and studied both catalytically and spectroscopically using the SFG spectroscopic technique. To allow these materials to be studied by SFG spectroscopy, they are supported on a substrate using a Langmuir–Blodgett technique, and the capping agent is removed by UV ozone treatment—a process also monitored by SFG spectroscopy (Figure 4). The results then obtained showed excellent parallels with those obtained on single-crystal surfaces as described above. Pt nanocubes with Pt(100)-like surfaces show the cyclohexyl intermediate in their SFG spectra and lead only to complete hydrogenation. In contrast, Pt nanocuboctahedra with both (100)- and (111)-like surfaces produce a mixture of cyclohexane and cyclohexene and have no CH_2 vibrational stretches indicative of the cyclohexyl intermediate in their SFG spectra.[8]

Freund and co-workers also used SFG spectroscopy to investigate CO adsorption on Pd single-crystal and nanocluster surfaces. Their results again illustrate the value of high-pressure and model-system studies using SFG spectroscopy, and in particular the extent to which conclusions drawn on the basis of experiments using single crystals can be extended to nanoparticles. They found that CO coexisted at both bridge and atop sites on Pd(111) crystal surfaces, while it adsorbs linearly on the well-faceted Pd clusters in the 3–6 nm size range at pressures of about 10^{-7} Torr. However, in the

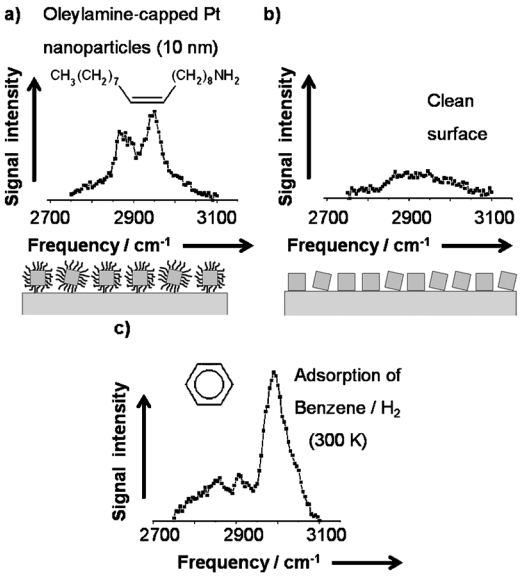

Figure 4. SFG spectra of the supported nanocubes: a) with capping agent; b) after UV ozone treatment showing the effective removal of capping agent; c) showing the absorption of surface species during the hydrogenation of benzene at 300 K.

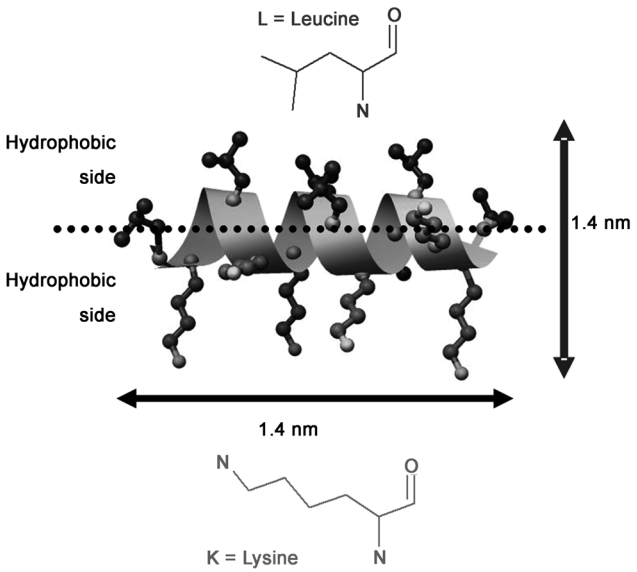

Figure 5. Schematic depiction of the LK14 peptide comprising both hydrophobic leucine and hydrophilic lysine units. Dimensions indicated were calculated using ideal helical bond angles and van der Waals radii.

higher-pressure (ca. 1 Torr) regime, binding of CO to both bridge and atop sites was seen for both Pd nanoclusters and Pd(111).[9]

In recent years, infrared–visible SFG spectroscopy has also been successfully applied to solid–liquid biointerfaces. Model peptides and even proteins have been studied on silica and polystyrene surfaces using SFG vibrational spectroscopy. Proteins are nature's enzymatic catalysts and are composed of amino acid "polymers" of various chain lengths. Amino acid chains induce a number of different secondary structures (for example α-helical and β-sheet). The interactions of amino acid units within these secondary structures, with surrounding molecules (e.g. H_2O), and with adsorbing surfaces are of importance for understanding their chemical behavior both in and ex vivo and offer the potential for understanding principles underlying enzymatic catalysis. SFG spectroscopy can be used to identify the interactions and orientations of proteins on a variety of surfaces. Because proteins are large and complex molecules, designed and synthesized model peptides offer systems that are a feasible starting point for studies in this area. The schematic depiction in Figure 5 shows such a synthetic peptide (LK14) in its α-helical structure. It is composed of leucine, which has a hydrophobic alkyl side chain, and lysine, which has a hydrophilic primary amine terminated side chain. The absorption of this peptide on the solid–liquid interface with silica and polystyrene surfaces produces a striking result. On the silica surface (which contains OH functionalities) an N–H stretch is observed in the SFG spectrum; this band can be attributed to the alignment of the peptide on the surface, bringing the hydrophilic lysine units towards the surface, where they can be detected by SFG spectroscopy (Figure 6). In contrast, on polystryrene (hydrocarbon) surfaces, the hydrophobic leucine units oriented toward the surface, generating C–H stretches

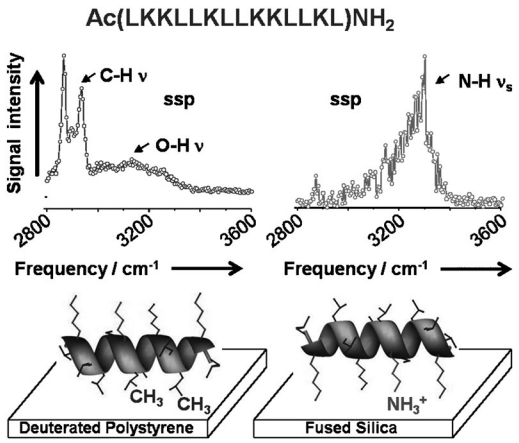

Figure 6. SFG spectra of LK14 solution adsorbed onto fully deuterated polystyrene (left) and fused silica (right). In the former the CH, CH_2, and CH_3 peaks dominate, while for the silica case the N–H stretching mode is the only dominant peak, thus indicating that it is these functionalities that are most closely associated with the surface, as depicted schematically below each spectrum. "ssp" denotes the orientation of the electronic vector of each polarized light beam (visible, ir and SFG) with respect to the reflecting surface.

in the SFG spectra instead (Figure 6). Although perhaps predictable, the ability to monitor such interactions in this way signals the possibility of being able to apply this technique to increasingly complex systems in which the dominant interactions are not clearly understood.[10]

The adoption of SFG vibrational spectroscopy in this field has already included surface studies of a number of more complex proteins. In our laboratory, the surface-concentration dependence on the binding geometry and molecular configuration of proteins such as lysozyme, fibrinogen, and

bovine serum albumin has been explored.[11] Similar studies at the protein–surface and protein–membrane interfaces have also recently been reported by several other investigators. Dreesen and co-workers studied the molecular recognition between avidin proteins and biocytin molecules and showed by SFG vibrational spectroscopy drastic changes in the C–H and N–H spectral regions of biocytin upon adsorption of avidin.[12] Yan and co-workers studied the conformational changes of amyloid proteins upon interaction with lipid membranes and found SFG vibrational signatures of the misfolding into β sheets of otherwise structureless amyloids upon adsorption onto lipid surfaces.[13] Similarly, experiments on carbohydrate-assisted enzyme immobilization on phospholipid membranes have been carried out using SFG spectroscopy, revealing correlations in the sulfate spectral region and the molecular configuration at the triphase boundary of this complex system.[14] Even nucleic acids have been studied using this approach: self-assembled monolayers of DNA strands on silica substrates were observed to adopt different structures in the presence of alkali- and alkaline-earth-metal cations depending on the DNA–cation affinity.[15] The authors of this work suggested that this result provides an attractive route for the design and fabrication of biosensors.

Overall, SFG spectroscopy has been used to provide detailed insight into reaction pathways, intermediates, and structure selectivity of catalytic systems during chemical change on both model single-crystal and nanoparticle surfaces as well as to probe the behavior of biological materials at interfaces—all phenomena which could not be observed without studying the systems under their relevant active conditions.

3. Scanning Tunneling Microscopy (STM)

Since the first demonstration of an HPSTM in situ reactor in our research group in 1992,[16] we have observed a number of changes working at elevated pressures, which are pertinent to the conditions under which real catalytic reactions occur. The initial HPSTM conducted in our research group was achieved by filling the STM chamber (separated from the rest of the vacuum system by a valve) with the reactive gas mixture.[16] Changes in the reactive gas mixture with time could also be monitored by mass spectrometry, effectively making this chamber into a batch reactor system. In this way, it was possible to see adsorbates under reaction conditions. A particularly illustrative study carried out in this mode was the hydrogenation of cyclohexene, which was conducted on a Pt(111) single crystal in 200 mTorr H_2 and 20 mTorr cyclohexene at room temperature.[17] Imaging was conducted as the gas composition was monitored with time using mass spectrometry. As shown in Figure 7a, under the reactive conditions, that is, where cyclohexene is being hydrogenated to cyclohexane (and a trace amount of benzene dehydrogenation side product), no surface order can be detected by STM. This result indicates the mobility or rapid diffusion of the adsorbates. In contrast, if a small partial pressure of carbon monoxide (5 mTorr) is present (Figure 7b), the reaction is poisoned and cyclohexane remains unreacted. STM shows

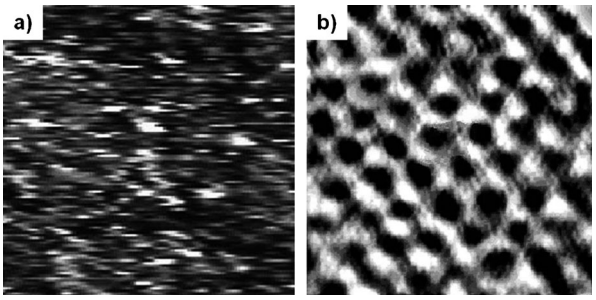

Figure 7. 90 Å × 90 Å images of Pt(111): a) in the presence of 20 mTorr cyclohexene and 200 mTorr H_2 at room temperature and under conditions in which the dehydrogenation product is simultaneously observed. No surface order can be discerned, but mobile adsorbate species are present that give rise to streaks as they are partially imaged by the scanning tip. b) Under the same conditions as in (a) but with the addition of 5 mTorr CO, which poisons the surface, displacing the cyclohexene and forming the stable hexagonal structure observed—no dehydrogenation reaction is seen.

that this poisoning is the result of preferential CO binding to the surface in the expected structure for CO on Pt(111).[18]

It could also be observed by STM that operating at a lower partial pressure of H_2 (1:1 with respect to cyclohexane), an immobile π-allyl species (cyclohexene which is partially dehydrogenated on the surface) is observed—just as with pure cyclohexene.[17] However, the observation of this stable surface species is entirely consistent with analysis of the composition of the reactive gases, which suggests no conversion of cyclohexene to either cyclohexane or benzene. Our group also observed a very similar CO poisoning effect with ethylene (rather than cyclohexene) as the hydrogenation reactant.[19]

Another significant advantage of STM is that it can be used to monitor both the molecular reactants adsorbed on a surface and the topology of the surface itself, in contrast to SFG spectroscopy described above, which can only interrogate the adsorbed reactants (although it can, of course, provide more detailed information about the bonding within them). Several examples have been reported for the reconstruction of single-crystal surfaces under relatively high-pressure conditions (near atmospheric pressure) in reactive gases. Besenbacher and co-workers used HPSTM to observe that a Cu(110) single crystal forms a (2×1) "missing row" only once 2 mbar or more of H_2 had been admitted to the sample chamber[20]—very different from the flat structure observed in the vacuum. Frenken and Hendriksen also used HPSTM to show CO restructuring of a Pt(110) surface with increasing pressure up to 1.25 bar; they observed a lifting of the vacuum structure to form much coarser steps.[21] Examples of adsorbate-induced reconstructions have been known for some time and are the simple result of the adsorbate–substrate bond formed on chemisorption providing a thermodynamic driving force that yields a different arrangement of substrate atoms at the surface. The observation of their occurrence in some systems only at elevated pressures can be understood straightforwardly as an extension of this thermodynamic equilibrium: the adsorbate coverage will be higher at higher pressure and includes the potential for weakly

adsorbed species to also be present—the number of adsorbate–surface interaction energies is therefore greater and thus inevitably more likely to also favor a different thermodynamic equilibrium structure of the surface atoms of the substrate.

Using a recently designed HPSTM system,[22] our group has observed dramatic and reversible reconstruction effects on Pt stepped surfaces with varying CO pressure.[23] In this setup, the STM body, STM tip, and sample are all placed in a small reaction vessel (ca. 19 cm^3) within the much larger overall UHV apparatus (Figure 8).[22]

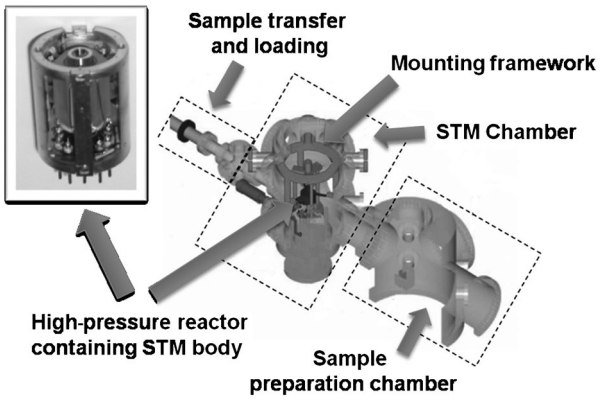

Figure 8. Schematic depiction of a high-pressure reactor specially mounted within an overall vacuum system and containing the STM body. The inset shows a photo of the high-pressure cell.

This system overcomes many of the previous limitations, such as large volumes of reactant gases and limits in sample heating, reactant-gas pressure, and spatial resolution. In this study, two highly stepped Pt surfaces, (332) and (557), were investigated with HPSTM for varying pressures of CO.[23] Such stepped surfaces serve as good model systems for small nanoparticle catalysts, as both contain a high density of edge and vertex sites. The most dramatic effect is observed on the Pt(557) surface and shown in Figure 9 (similar reconstruction effects were also observed on the Pt (332) single crystal). On introduction of a small pressure of CO (1×10^{-8} mbar), a typical adsorbate-induced reconstruction is observed in which the steps broaden and the step height doubles (Figure 9b).

However, when the CO pressure is increased to the 1 Torr range (much closer to the operational range of many catalytic systems) a dramatic change is seen in the formation of small triangular clusters (Figure 9c). Complimentary ambient-pressure XPS measurements (a technique described in more detail below) show that the CO coverage at 0.5 Torr is approximately double that of adsorbed CO at 1×10^{-8} mbar and corresponds to a 1:1 ratio of CO molecules to atoms in the original surface structure. Under these conditions DFT calculations support the formation of such clusters. The thermodynamic driving force can be understood in terms of cluster formation reducing the unfavorable repulsive interactions between CO molecules on the crowded surface. Furthermore, when the CO pressure is dropped back to 1×10^{-8} mbar after exposure at 1 Torr, the triangular clusters

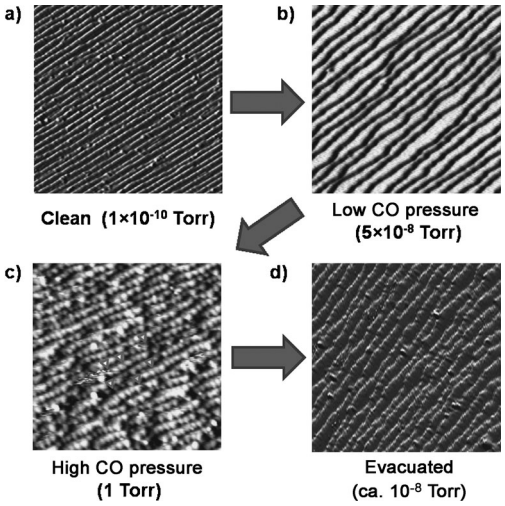

Figure 9. 400 Å×400 Å images of Pt(557) surface: a) in ultrahigh vacuum with a background pressure of 1×10^{-10} Torr; b) showing broadening and increased step height after admission of ca. 5×10^{-8} Torr CO; c) showing restructuring to triangular clusters (several examples marked) during exposure to 1 Torr CO; and d) return to stepped structure occurring reversibly on removal of CO atmosphere to vacuum (ca. 10^{-8} Torr).

disappear and the sample returns to a morphology similar to that observed after the clean sample is exposed to 1×10^{-8} mbar of CO (Figure 9d). APXPS also indicates that the CO coverage decreases to the lower coverage expected. Therefore, on cycling the system from low CO pressure to high CO pressure, a fully reversible restructuring process is observed (with only minor losses in the degree of order of the surface morphology at low CO pressure after many repeated cycles). Since this behavior depends on the CO coverage in equilibrium with the surrounding gas, it is a good demonstration of the effect of shifting the thermodynamic equilibrium structure by increasing the number of adsorbate–surface interactions outlined above. The reversible nature of this effect also underlines the importance of studying surface catalysis during reactions or near reaction conditions to understand the morphology that is really present during a reaction.

In addition to working at the solid–gas interface under reaction conditions, operation of scanning tunneling microscopes has also been pioneered for examining the buried solid–liquid interface. Initially, this application focused predominantly on the field of electrochemical surface science, where the tip also functioned as an electrode.[24] More recently, however, it has been applied to directly image a single molecular reaction—the oxidation of a manganese porphyrin on a Au(111) surface, which may then subsequently oxidize an alkene to an epoxide as detected by gas chromatography.[25] Although this feat is impressive, many challenges still remain with this approach, in particular the limited solvent choices. The solvent must usually have a high boiling point to maintain a stable liquid phase and a low polarity so as not to interact strongly with the electric field at the tip. Additionally, the example of a surface porphyrin oxidation is selected because the timescale is on the order of many

seconds, but this long reaction time is seldom found for chemical reactions of interest, and time resolution remains a definite challenge of this technique.[26] Advances in these areas will undoubtedly reveal even more information about the surface interactions occurring in these systems by interrogating them under reaction conditions. However, overall it is apparent that HPSTM is a technique with proven application to both solid–gas and solid–liquid interfaces that readily monitors reversible changes only present under the conditions at which the chemical phenomena of interest are actually occurring.

4. Ambient-Pressure X-ray Photoelectron Spectroscopy (APXPS)

Conventionally, the use of the photoelectron effect to produce emission spectra corresponding to electronic energy levels using X-rays has been an ultrahigh-vacuum technique, in which the emitted electrons are quickly absorbed before escaping any form of buried interface. In recent years, advances in both vacuum and analyzer technologies in conjunction with the use of high-flux X-ray photon sources provided by synchrotrons have allowed the development of specialist XPS systems that can be operated at higher pressures. This high-pressure operation is achieved by a series of powerful differential pumping systems between the sample and the analyzer, such that the reactant gases are only at reaction pressure in the immediate vicinity of the surface, a metal sample cone with a narrow orifice admitting photoelectrons and only a small flow of gas into the first differentially pumped chamber (Figure 10). For instance, at the synchrotron facility used in the experiments outlined below

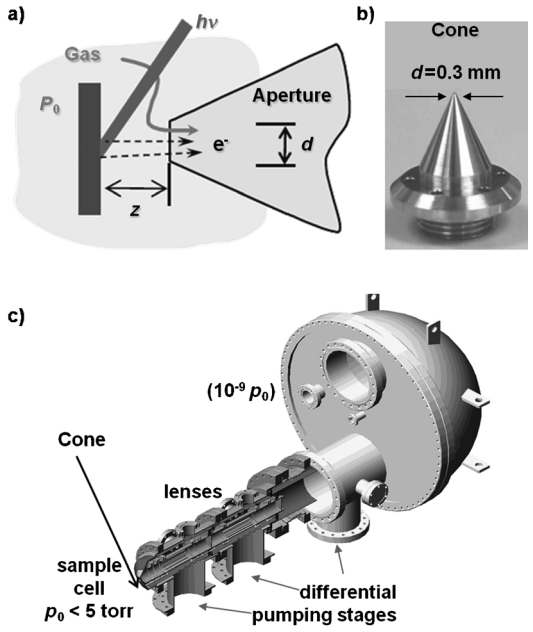

Figure 10. a) Diagram of the "sample-first" aperture geometry typically used for APXPS experiments; b) sample cell "first aperture cone"; c) schematic cross section of the electrostatic lens, differential pump, and energy analyzer setup.

(Advanced Light Source, Berkeley, CA, USA) gas pressures up to approximately 5 Torr are accessible. In this range, a number of solid–gas heterogeneous catalytic reactions (e.g. with NO/CO or CO/H_2 as reactants) are found to be catalytically operative, and thus exploration by XPS in situ has considerable potential for offering important mechanistic insights at the molecular level.

In classical XPS, core energy levels of elements are excited by (usually) Al or $Mg_{K\alpha}$ laboratory-source-generated X-rays, and ejected photoelectrons travel in vacuum to an electron-energy analyzer. The typical depth probed depends on the kinetic energy of the ejected photoelectrons, which, when using a laboratory source, are in the 8–20 Å range for most transition metals. The kinetic energy of the emitted electron is determined by the element-specific energy of the atomic core energy level being analyzed, and hence for a fixed-frequency laboratory source, the probed sample depth is also fixed. Synchrotron sources, however, allow the incident X-ray energy to be varied over a considerable range, and thus emitted electron kinetic energies and the sample depth probed can also be tuned. Elemental and chemical compositions of surface regions in the 6–30 Å range can then be probed and mapped. This information is particularly useful under temperature and pressure conditions mimicking those of catalytically relevant reactions, obtainable by APXPS, where dynamic changes may be observed.

Recently, APXPS has been used to address a number of long-standing questions concerning the nature of surfaces under conditions of practical catalysis. A number of examples studied by our laboratory serve to illustrate the benefits of such work.

Rhodium is known to be an active catalyst for the oxidation of CO, but little was known about the nature of the surface under reaction conditions. By employing size-controlled Rh nanoparticles in conjunction with APXPS, questions regarding the possible role of Rh_2O_3 and structure sensitivities could be explored. APXPS investigation of the size-controlled Rh nanoparticles in the 2–11 nm size range has revealed a strong size correlation with the chemical composition of Rh on the surface. Under reaction conditions, small Rh nanoparticles (2 nm) exhibited the largest RhO_x contribution to their structure, while large Rh nanoparticles (11 nm) were predominantly metallic (Figure 11). In other words, for a given partial pressure of O_2, a RhO_x phase was thermodynamically dramatically favored for nanoparticles relative to bulk material. Complimentary catalytic measurements showed that small (oxidized) Rh nanoparticles are considerably more active than large ones (by a factor of ten in their turnover number per surface site), and in agreement with this finding, a strong size correlation with the activation energy was observed.[27]

As discussed above in reference to single-crystal in situ STM experiments, surface–adsorbate interactions are of intrinsic importance in heterogeneous catalytic reactions. Similarly, they should play a crucial role in determining the chemical and structural stability of nanoparticle catalysts. For bimetallic nanoparticles especially, both composition and particle architecture emerge as variables that have crucial influence over catalytic behavior. Atomic distribution in the

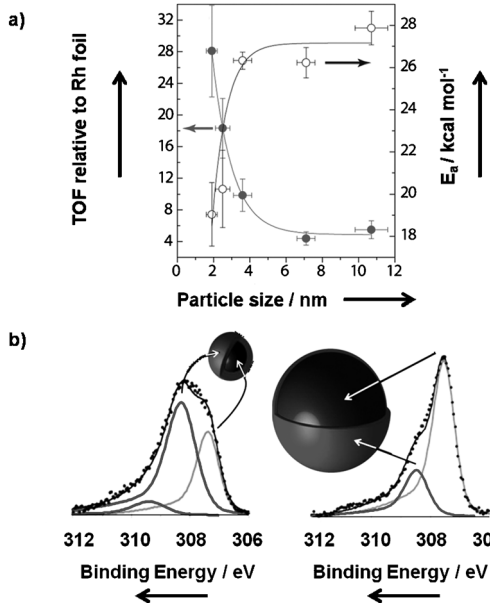

Figure 11. a) A plot of turnover frequency (TOF) relative to Rh foil (solid circles) and apparent activation energy (empty circles) for CO oxidation with varying Rh nanoparticle size; b) example XP spectra for 2 (left) and 7 nm (right) Rh nanoparticles showing oxidized (light gray) and reduced (dark gray) states of Rh. Catalytic screening was carried out under 50 Torr O_2 and 20 Torr CO (690 Torr He) at 200 °C. Apparent activation energy was measured in the 150–200 °C temperature range. The APXPS study was conducted at 100 mTorr O_2 and 40 mTorr CO reaction atmosphere at 200 °C. Rh 3d photoelectron kinetic energy ca. 200 eV. The oxide layers in the illustrations are drawn to scale based on APXPS results.

bulk material is predominantly determined by the nucleation and growth kinetics of bimetallic nanoparticles. In contrast, surface chemical and elemental composition can be considered to be much more dynamic and have been found to be altered dramatically by both thermodynamic and kinetic factors. In particular, the interplay of metal-surface free energy and the heat of adsorption of the reactive gas molecules can control these factors and lead to different reaction rates and reaction pathways. APXPS is currently a unique spectroscopic tool to explore this behavior of bimetallic nanoparticle catalysts in the presence of catalytically relevant pressures of reactive gases. In addition to the structure of the metal surface, adsorbate molecules interacting with the metal and co-adsorbed species can be observed using APXPS, thus allowing a complete picture of the surface at the atomic and molecular level to be drawn.

Rhodium–palladium alloy catalysts are commonly used in three-way catalytic converters (TWC) to reduce NO and simultaneously oxidize CO. Bimetallic nanoparticles comprising these metals have been considered promising candidates for the next generation of TWC catalysts; however, the phase behavior and stability of their binary alloys under the reaction conditions were poorly understood and posed a potential barrier to such application. To try to address this question, composition-controlled 15 nm $Rh_{1-x}Pd_x$ ($x = 0.2$–0.8) NPs were synthesized using colloidal chemistry and studied using APXPS under conditions in which the catalytic reaction could also be observed. By tuning the energy of the incident X-rays, a depth-profile analysis could be carried out. The results are shown in Figure 12, showing the equilibrium

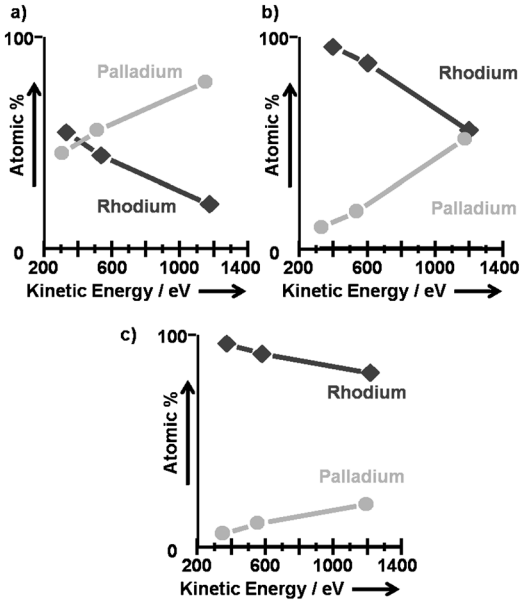

Figure 12. Dependence of rhodium and palladium atomic fractions of as-synthesized Rh_xPd_{1-x} nanoparticles ($x = 0.2$–0.8) measured at 25 °C in vacuum ($< 1 \times 10^{-8}$ Torr) as a function of photoelectron kinetic energy (bottom axis) for a) $Rh_{0.2}Pd_{0.8}$, b) $Rh_{0.5}Pd_{0.5}$, and c) $Rh_{0.8}Pd_{0.2}$. Measurements were made at photoelectron kinetic energies of approximately 350, 575, and 1200 eV, corresponding to probing depths of approximately 0.7, 1.0, and 1.6 nm, respectively, below the surface of the 15 nm nanoparticles.

atomic and chemical composition of nanoparticles with depth in the surface region of the nanoparticles (ca. 1.5 nm). In all cases, the $Rh_{1-x}Pd_x$ NPs initially (without reactive gases present) have Rh-rich shells (97 atomic % Rh for the $Rh_{50}Pd_{50}$ NPs). At 1.5 nm below the surface, however, the Rh:Pd ratio returned to that of the bulk nominal compositions in all cases (i.e., the $Rh_{50}Pd_{50}$ NPs exhibited exactly 50 atom % Rh for photoelectrons emitted from 1.5 nm below the surface). These same bimetallic nanoparticles were exposed to oxidizing (NO, O_2) gases, reducing (H_2) gas atmospheres, or catalytic mixtures (stoichiometric mixture of NO and CO) and studied by APXPS (gas pressures ca. 0.1 Torr). It was found that at a temperature as low as 300 °C all the $Rh_{1-x}Pd_x$ NP compositions showed a marked surface enrichment of Pd under the catalytic conditions of 1:1 NO:CO. Similarly, reducing gas caused Pd enrichment in the surface regions to an even greater extent (60 % more Pd than measured in vacuum). On returning to oxidizing (NO or O_2) gas, the Rh again segregates toward the surface and the Pd disappears into the bulk (Figure 13). Furthermore, this adsorbate-induced switching of the surface metal composition could be cycled repeatedly by switching between the different gas atmospheres—a fact that again indicated the importance of studying such systems under reaction conditions. In the same vein, it should also be noted that the initial surface compo-

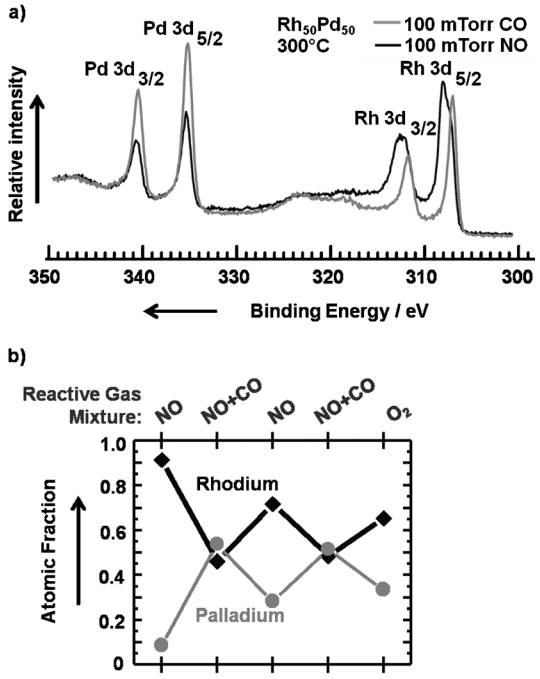

Figure 13. a) Typical XP spectra of Rh 3d and Pd 3d core levels for $Rh_{0.5}Pd_{0.5}$ nanoparticles (ca. 15 nm) collected in 0.1 Torr NO (black) and 0.1 Torr CO (gray) at 300 °C; b) Evaluation of the atomic fractions of Rh (black) and Pd (gray) under oxidizing atmospheres (0.1 Torr NO or O_2) and reaction (0.1 Torr of both NO and CO) at 300 °C. X-ray energy used for stimulating photoelectron emission was 645 eV for both Rh 3d and Pd 3d core levels.

sitions of metals are restored on cooling down to room temperature or returning the sample to vacuum.

These APXPS observations are readily rationalized by this thermodynamic equilibrium interplay between metallic surface free energies (dominant in reducing conditions and in the absence of adsorbate molecules and less favorable for Rh surfaces) and the heat of adsorption for reactant gas molecules (NO has the larger heat of adsorption on Rh, and Rh_2O_3 formation is more favorable than PdO formation).[28,29]

Catalytically, a synergistic effect whereby RhPd bimetallic nanoparticles perform better than the pure Pd or pure Rh particles is observed. Moreover, the surface reactivity in the dissociation of NO to form oxide peaked for the nanoparticles with a 20 atomic % Pd bulk composition, which have most Rh in the surface regions as monitored by APXPS; some Pd sites for CO binding were retained. Thus, APXPS revealed the kinetically stable nanoparticle structures under the reactive gas atmospheres and also indicated an intriguing way to tune particle stability and surface reactivity. A similar although less dramatic effect was also observed for RhPt, while PtPd does not undergo such transformations. These results, however, are entirely consistent with these segregation effects being driven by an equilibrium between surface energies and the heat of adsorption of reactive gas molecules. Pd is favored in both cases and thus always dominates the surface.[28] A similar approach using APXPS has also been adopted to address questions about Au–Pd catalysis,[30] in particular with respect to its previously highlighted activity for CO oxidation.[31]

Others have also reported APXPS studies on model surfaces. Methanol oxidation was studied on elemental copper at various reactant stoichiometries at a total pressure of 0.6 mbar and at 400 °C.[32] APXPS was used to identify a strong correlation between the selectivity for formaldehyde monitored in situ and the presence of subsurface oxide in the metallic copper catalyst. This oxide was identified from two experiments, the first comparing the valence states with the oxygen core levels and the second using different photon energies to profile the oxide phase with sample depth.[32] Similarly, Kondoh and co-workers investigated NO adsorption on Pt(111) single-crystal surfaces at pressures near 1 Torr using APXPS. Their results showed that NO on Pt(111) adsorbs in both fcc-hollow (fcc = face-centered cubic) and atop geometries at pressures above 10^{-6} Torr, while it absorbs dominantly only on fcc-hollow sites at lower pressures. They also identified that NO adsorption on the Pt(111) surface at elevated pressures is irreversible.[33]

Overall, APXPS is a powerful tool for the study of surface chemical and elemental composition and of particular utility in profiling the behavior of systems in which several possibilities exist for the active state of the catalyst that may only be adopted under reaction conditions, whether that is the presence of oxides or the transformation of surface metal composition in bimetallic materials.

5. X-ray Absorption (EXAFS and NEXAFS) Spectroscopies

In addition to APXPS, these two further techniques, both based on the photoelectron effect and achievable using synchrotron radiation, can be used under reaction conditions for the exploration of surface-catalyzed processes. Both are essentially different components of the same spectral phenomenon but are utilized differently to betray different information. Both EXAFS and NEXAFS spectroscopy are simply measurements of the energy dependence of the photoabsorption coefficient (as described by Beer's law, just as for any other region of the electromagnetic spectrum). Consequently, these techniques are very element-specific: the incident photons are absorbed as the result of electron-energy transitions, which are different for the core levels of different elements. The most common transition is the straightforward ionization of a core electron, but in the region near this ionization threshold or "edge" there may also be dipole-allowed transitions from core levels to Rydberg states or antibonding orbitals, and it is these transitions that give rise to the so called "near-edge" (NEXAFS) spectrum.[34] This region of the spectrum and the adsorption edge itself can therefore give information about chemical environment, such as formal oxidation state, symmetry, or local charge distribution. Photoelectrons that are instead emitted completely from the atom may be subject to backscattering effects with the electron clouds around their immediate and near neighbors. It is these scattering effects that are observed as oscillations that make up the "extended X-ray absorption fine structure" (EXAFS) spectrum to the high-energy side of the ionization threshold. Since such backscattering effects result from the

atoms neighboring the absorber atom, this spectral region provides information about the local environment: the number and type of coordinating atoms and the distances to these neighbors.[35]

Measurement of photoabsorption in general is carried out by simply monitoring a sample's transmission of the relevant electromagnetic wave versus the intensity incident on the sample. X-ray absorption measurements may be made by this transmission method, but for both dilute samples and those where surface-sensitive information is sought, indirect methods may sometimes be advantageous. In particular, X-ray fluorescence, Auger electron emission, and total-electron-yield measurements can all be utilized to indirectly monitor X-ray absorption (Figure 14).

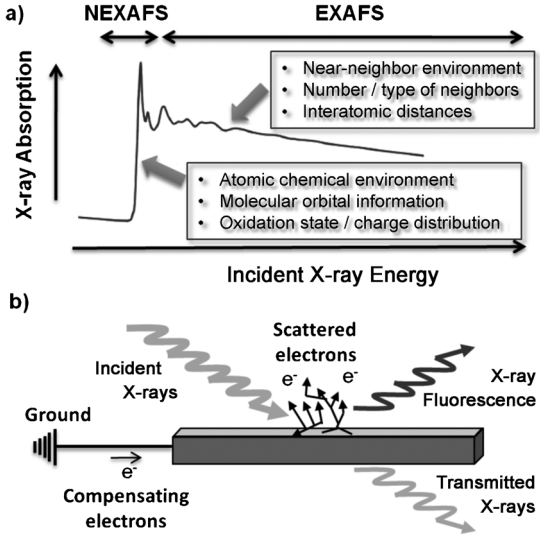

Figure 14. a) Typical X-ray absorption spectrum showing NEXAFS and EXAFS region features; b) schematic depiction showing possible signals used for detection of X-ray absorption spectra (both NEXAFS and EXAFS).

The detection method used has two important consequences: 1) the depth into the sample that is probed (since incident X-rays can typically penetrate to any realistic sample depth, they are unlikely to limit which part of the sample is being probed) and 2) the ability to record measurements in situ. Both of these factors are pertinent to the focus of our present discussion. These indirect measurement methods rely on the fact that the emission of a photoelectron from a core level within an atom leaves a "core hole" behind. Higher-energy electrons can then decay to fill this hole either by X-ray fluorescence or the emission of an Auger electron.[36] The dominance of these two effects is controlled by the absorption edge being studied (Auger emission dominates for small atomic numbers ($Z \lesssim 30$ for K shells), while fluorescence is the major decay process for larger atoms).[37] Since fluorescence produces X-rays, which are relatively weakly absorbed by other atoms, these can escape from the bulk of the material being sampled. Fluorescence detection is therefore classified as a "bulk" measurement. Equally, the use of emitted fluorescence X-rays has the advantage that the X-rays can be collected through a liquid or a high-pressure gas phase (through which the emitted X-rays, unlike electrons,[38] can penetrate). In contrast, if the X-ray absorption is quantified using Auger electrons, or more realistically Auger electrons and secondary scattering electrons, together called total electron yield (TEY), the escape depth of the electrons makes the spectra obtained relatively sensitive to surface phenomenon.[34] As we will see in the examples that follow, these electrons may be either be: 1) collected from near the sample surface before being absorbed by scattering events or 2) measured as part of a complete electric circuit. The second case is made possible since when electrons are emitted from the sample, a compensating current (which can be measured using a picoammeter) must flow between the sample and ground.

5.1. Near-Edge X-ray Absorption Fine Structure

We have recently demonstrated the use of TEY measurement recorded using the compensation current between the sample and ground to record NEXAFS spectra of Co and PtCo nanoparticles in oxidizing or reducing atmospheres at atmospheric pressure.[39] Measurement of the TEY current in this way (by measuring the current to the sample rather than collecting the emitted electrons) overcomes the inherent limitations of emitted electrons that will inevitably be susceptible to absorption by inelastic scattering when the surface studied is at a buried interface, such as a solid–gas or solid–liquid catalyst under reactions conditions. The atmospheric pressure reactor in which this work was carried out is depicted in Figure 15.

It is separated from the UHV system in which it is located by a Si_3N_4 membrane window for the admission of X-rays. The metal-nanoparticle catalyst is then deposited as a Langmuir–Blodgett film on a conducting gold foil. Crucially, the

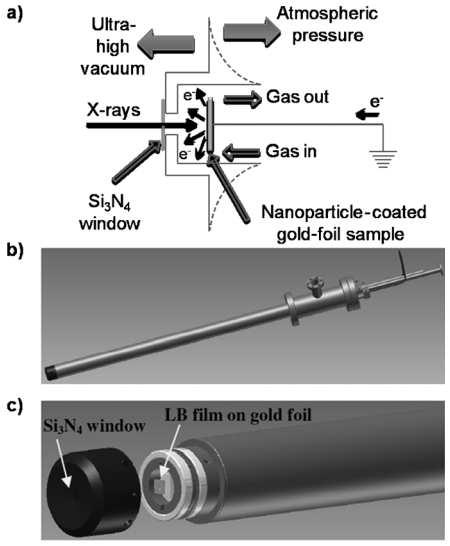

Figure 15. a) Schematic depiction of the in situ gas-flow NEXAFS cell configuration; b, c) 3D visualizations of the in situ NEXAFS cell depicting arrangement of the Langmuir–Blodgett nanoparticle-film sample holder in relation to the X-ray window.

nanoparticle layer present on the gold foil is comprised of particles of approximately 4 nm size and thus is comparable to the escape depth of the TEY electrons, thus ensuring that measurement of the compensating flow of electrons into the sample accounts for all of the TEY electrons produced—they are not simply scattered back by other areas of the sample. This sample is then located within a few millimeters of the window within the atmospheric-pressure reaction cell, thus minimizing any absorption by the gas phase. Use of this configuration allowed NEXAFS of the cobalt L edge to be obtained for specially prepared Co and $Co_{0.5}Pt_{0.5}$ nanoparticles of 4 nm (Figure 16a shows typical spectra obtained). By comparison with known reference states of Co, the amount of Co and Co^{2+} present in the samples was determined for the two types of nanoparticles while in an oxidizing atmosphere at 1 bar.

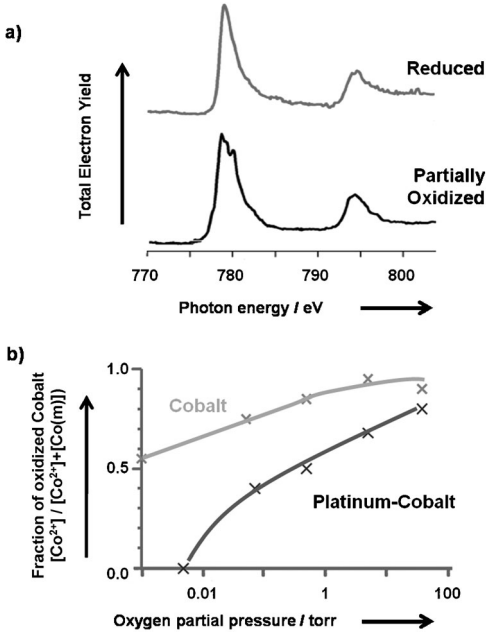

Figure 16. a) Typical Co L-edge NEXAFS spectra of a 4 nm CoPt nanoparticle model catalyst in both fully reduced and partially oxidized states. b) Fraction of cobalt atoms present as oxidized Co^{2+} with increasing oxygen partial pressure as determined from in situ NEXAFS spectra. PtCo bimetallic particles are more oxidation-resistant than the equivalent pure Co particles (lines are added for guidance only). Co(m) denotes metallic cobalt.

As can be seen from Figure 16b, the presence of platinum decreases the susceptibility of the nanoparticles to oxidation relative to those without Pt. In situ reduction in H_2 also indicated that the PtCo particles could be much more readily reduced than their pure Co counterparts. In both environments the ability to study the oxidation state and oxidation resistance of these catalysts in the presence of reactive gases provides important insights into their likely behavior in processes to which cobalt catalysts are typically applied, such as CO oxidation and Fischer–Tropsch synthesis. A very similar experimental setup has also been used by others to study the oxidation state of Co nanoparticle model catalysts of varying size in different reactive gas atmospheres.[40]

Total-electron-yield NEXAFS spectra may also be acquired by careful positioning of a collector plate or grid in the vicinity of the sample to collect the electrons emitted from the sample. Such a setup was used by Schlögl and co-workers to investigate MeOH oxidation over copper foil[41] and later over a Co(0001) single crystal[42] under reaction conditions. In this way they were able to elucidate the extent of oxidation in the metal structure and rationalize complimentary catalytic measurements accordingly. They also exploited this setup to study the adsorption of acrolein on silver for hydrogenation reactions.[43] By using both oriented single crystals and nanoparticle model catalysts, this study was able to exploit symmetry-selection rules of NEXAFS spectroscopy, which for the single-crystal case result in an intensity variation with photon incidence angle.[44] This relationship allowed determination of the orientation of the surface species under reaction conditions (0.01 mbar acrolein in 7.5 mbar H_2).[43] Again, recording spectra under reaction conditions affords valuable insights into the influence of catalyst structure and pressure on the adsorption of acrolein during the reaction and the reaction selectivity observed towards propionaldehyde under these conditions. It also highlights the suitability of the low-energy X-ray region to be exploited for studying the reactants as well as the catalyst material. The fine structures of the C, N, and O near K edges are all very sensitive to local molecular structure and bonding.

Other detection techniques can also be used to record NEXAFS spectra under reaction conditions. Absorption between incident and transmitted X-rays was measured for a Rh/Al_2O_3-catalyzed methane partial oxidation reaction.[45] In this instance transmission was selected to allow additional 2D spatial information to be obtained, thus providing a map of the catalyst bed. Fluorescence yield detection was adopted by Bokhoven et al. for an interesting study to try and elucidate the mechanism for the controversial gold-catalyzed CO oxidation reaction.[46] They carried out the reaction stepwise in different reactive gas atmospheres, demonstrating that oxygen is activated by charge transfer from d-band electrons of the catalytically active small gold particles.

5.2. Extended X-ray Absorption Fine Structure

Perhaps because it is often used with higher-energy X-ray absorption edges that can penetrate a wide range of reaction-vessel materials and windows, EXAFS spectroscopy has been applied more extensively to the study of catalytic processes under reaction conditions. It is most often applied in transmission mode. In particular, EXAFS spectroscopy offers an excellent probe of coordination number and bonding environment (including oxidation state) and thus has been used to characterize the chemical state of catalysts and their active sites under reaction conditions in a diverse array of systems. Quite often it is used simultaneously with gas chromatography or mass spectrometry to probe an actual flow reactor in real time. One such example is the study of copper-catalyzed MeOH oxidation in a quartz capillary reactor.[47] This real-time acquisition of spectra is often referred to as quick-EXAFS or 'QEXAFS' spectroscopy. Similarly, using the

European Synchrotron Radiation Facility in Grenoble, Rh K-edge EXAFS spectra recorded under reaction conditions were able to demonstrate that the change in selectivity between N_2 and N_2O formation during NO_2 reduction resulted from the absence and presence, respectively, of oxidized sites on the Rh metal.[48] At the same facility, this approach has now been extended to obtain gas-phase EXAFS spectra at up to 18 bar for the Co-catalyzed Fischer–Tropsch synthesis, a reaction of significant industrial importance.[49] This same approach has also been applied to liquid-phase reactions[50] and even to the study of oxidation reactions in supercritical CO_2 at 150 bar.[51] To date, all the EXAFS spectroscopy studies described have been recorded using the transmission method, but it is equally possible to use the same indirect methods described above to measure EXAFS spectra. Indeed, one of the earlier examples of in situ EXAFS spectroscopy (looking at the active state of the catalyst in Cu-catalyzed methanol synthesis) used a form of total-electron-yield measurement.[52,53] In this study, the emitted electrons were used to ionize helium gas (present in the reaction gas mixture) to give an ionization cascade between the sample and a strongly biased anode; the gas therefore multiplies rather than diminishes the total-electron-yield signal. Recently EXAFS spectra of a Pd nanoparticle model catalyst in a recirculating batch reactor were recorded using fluorescence detection through Kapton windows.[54,55] In this example, liquid-phase Suzuki coupling was studied, where low concentrations of Pd catalyst are typically employed and thus fluorescence-yield detection offers the considerable advantage of sensitivity to low concentrations that may not easily be detected as a fraction of the overall X-ray intensity. Further details of the application of EXAFS spectroscopy under catalytically relevant conditions have been described elsewhere.[56]

In our laboratory we have recently developed an in situ EXAFS spectroscopy cell for use with the Advanced Light Source synchrotron facility. The heated reaction cell allows hard X-ray edge absorption spectra to be acquired in both transmission and fluorescence detection modes, thus providing sensitivity to elements present in both high and low concentrations in the reaction system. We are currently exploiting this setup to study dendrimer-supported catalysts in the liquid phase comprised of specifically tailored metal nanoparticles, which (as recently reported) have the potential to allow heterogenizing of homogeneous catalysis by alteration of the properties of low-coordination metal sites.[57] In this case, characterization of the active material under reaction conditions is clearly vital to understand more fully the catalyst's mode of action.

Overall, the examples given of adaptation of these two X-ray absorption spectroscopies for use under reaction conditions again highlight the very different structure, composition, and dynamics seen at interfaces on the molecular level when they are studied under conditions relevant to the chemical change of interest.

6. Other in Situ Techniques

In addition to the insights gained above, a number of other techniques have been and are being developed elsewhere to study surfaces under reaction conditions and have provided information demonstrating that they, too, are promising additions to complement the tools described above. Examples include in situ grazing incidence small-angle X-ray scattering/X-ray diffraction (demonstrated for $Pd_8Ni_{92}(110)$ crystal surfaces under H_2 and butadiene/H_2 mixtures in the 1 Torr pressure regime at 500 K);[58] polarization-modulation infrared reflection absorption spectroscopy (e.g., studies of AuPd-(100) crystal surfaces in the 1 Torr pressure regime and at elevated temperatures);[59] and microRaman spectroscopy (demonstrated for solid-oxide fuel cell Ni/yttria-stabilized zirconia (YSZ) electrocatalysts under working gas conditions and at 1000 K).[60] In situ solid-state NMR spectroscopy has also been used to probe reaction intermediates in a number of catalytic reactions, as is described in some detail elsewhere.[61] One other very noteworthy case is environmental transmission electron microcopy (E-TEM). Although it is, again, conventionally limited to ultrahigh vacuum for technical reasons, advances in vacuum technology have made pressure- and temperature-controlled atmospheres possible.[62] TEM offers the possibility of both imaging and spectroscopy in one instrument, and thus its application under reaction conditions may allow many new insights into the true behavior of catalytically active buried interfaces. Both the imaging and spectroscopic capabilities have been demonstrated with reactive gases at pressures in the 1 Torr region and temperatures as high as 1200 °C with little loss of contrast and resolution.[63] Specific examples investigated to date include the stability of MgO nanocubes with water vapor (0.4 Torr),[64] the redox behavior of CeO_2-based oxide catalysts in high-temperature H_2 (0.5 Torr),[65] and reversible morphology changes of Pt nanoparticles on changing from oxidizing to reducing gas environments.[66] Even structural and morphological evolution of nanoparticle catalysts under near-catalytic wet-chemical conditions have been studied using this technique for a Co–Ru/TiO_2 hydrogenation polymerization catalyst.[67]

7. Conclusions and Future Perspectives

The development of this toolbox of techniques has permitted studies of buried interfaces under reaction conditions and has already allowed new environment-induced surface phenomena, which were previously unknown, to be uncovered—in adsorbate and surface structure, composition, and dynamics. The reversible nature of many of the changes described also highlights the importance of striving to study such effects under the conditions of the actual reaction, as considerable changes are seen on moving away from the reaction environment. By employing model catalysts and these in situ techniques in combination, the goal of acquiring a molecular picture of the mechanisms at play in a range of interfacial phenomena can finally be realized. With time and the advent of increasingly advanced instrumentation designed

with this end in mind, we undoubtedly have much more to learn as we become able watch surface phenomena at both higher-pressure gas–solid and even liquid–solid interfaces on the molecular level.

Received: December 27, 2011
Published online: May 27, 2011

[1] D. W. Goodman, *Chem. Rev.* **1995**, *95*, 523.
[2] G. A. Somorjai, J. Y. Park, *Top. Catal.* **2008**, *49*, 126.
[3] G. A. Somorjai, J. Y. Park, *Angew. Chem.* **2008**, *120*, 9352; *Angew. Chem. Int. Ed.* **2008**, *47*, 9212.
[4] X. D. Zhu, H. Suhr, Y. R. Shen, *Phys. Rev. B* **1987**, *35*, 3047.
[5] Y. R. Shen, *Nature* **1989**, *337*, 519.
[6] P. S. Cremer, X. Su, Y. R. Shen, G. A. Somorjai, *J. Am. Chem. Soc.* **1996**, *118*, 2942.
[7] X. Su, K. Kung, J. Lahtinen, R. Shen, G. Somorjai, *Catal. Lett.* **1998**, *54*, 9.
[8] K. M. Bratlie, H. Lee, K. Komvopoulos, P. Yang, G. A. Somorjai, *Nano Lett.* **2007**, *7*, 3097.
[9] H. Unterhalt, G. Rupprechter, H.-J. Freund, *J. Phys. Chem. B* **2002**, *106*, 356.
[10] O. Mermut, D. C. Phillips, R. L. York, K. R. McCrea, R. S. Ward, G. A. Somorjai, *J. Am. Chem. Soc.* **2006**, *128*, 3598.
[11] J. Kim, G. A. Somorjai, *J. Am. Chem. Soc.* **2003**, *125*, 3150.
[12] L. Dreesen, Y. Sartenaer, C. Humbert, A. A. Mani, C. Méthivier, C.-M. Pradier, P. A. Thiry, A. Peremans, *ChemPhysChem* **2004**, *5*, 1719.
[13] L. Fu, G. Ma, E. C. Y. Yan, *J. Am. Chem. Soc.* **2010**, *132*, 5405.
[14] T. M. Nobre, H. de Sousa e Silva, R. P. M. Furriel, F. A. Leone, P. B. Miranda, M. E. D. Zaniquelli, *J. Phys. Chem. B* **2009**, *113*, 7491.
[15] H. Asanuma, H. Noguchi, K. Uosaki, H.-Z. Yu, *J. Am. Chem. Soc.* **2008**, *130*, 8016.
[16] B. J. McIntyre, M. B. Salmeron, G. A. Somorjai, *Catal. Lett.* **1992**, *14*, 263.
[17] M. Montano, M. Salmeron, G. A. Somorjai, *Surf. Sci.* **2006**, *600*, 1809.
[18] E. Kruse Vestergaard, P. Thostrup, T. An, E. Lægsgaard, I. Stensgaard, B. Hammer, F. Besenbacher, *Phys. Rev. Lett.* **2002**, *88*, 259601.
[19] D. C. Tang, K. S. Hwang, M. Salmeron, G. A. Somorjai, *J. Phys. Chem. B* **2004**, *108*, 13300.
[20] L. Österlund, P. B. Rasmussen, P. Thostrup, E. Lægsgaard, I. Stensgaard, F. Besenbacher, *Phys. Rev. Lett.* **2001**, *86*, 460.
[21] J. Frenken, B. Hendriksen, *MRS Bull.* **2007**, *32*, 1015.
[22] F. Tao, D. Tang, M. Salmeron, G. A. Somorjai, *Rev. Sci. Instrum.* **2008**, *79*, 084101.
[23] F. Tao, S. Dag, L. W. Wang, Z. Liu, D. R. Butcher, H. Bluhm, M. Salmeron, G. A. Somorjai, *Science* **2010**, *327*, 850.
[24] R. Helbig, A. Dakkouri, M. Dietterle, D. Kolb, in *Festkörperprobleme*, *Vol. 36*, Springer, Berlin, **1996**, p. 1.
[25] B. Hulsken, R. Van Hameren, J. W. Gerritsen, T. Khoury, P. Thordarson, M. J. Crossley, A. E. Rowan, R. J. M. Nolte, J. Elemans, S. Speller, *Nat. Nanotechnol.* **2007**, *2*, 285.
[26] J. A. A. W. Elemans, *Mater. Today* **2009**, *12*, 34.
[27] M. E. Grass, Y. Zhang, D. R. Butcher, J. Y. Park, Y. Li, H. Bluhm, K. M. Bratlie, T. Zhang, G. A. Somorjai, *Angew. Chem.* **2008**, *120*, 9025; *Angew. Chem. Int. Ed.* **2008**, *47*, 8893.
[28] F. Tao, M. E. Grass, Y. Zhang, D. R. Butcher, F. Aksoy, S. Aloni, V. Altoe, S. Alayoglu, J. R. Renzas, C.-K. Tsung, Z. Zhu, Z. Liu, M. Salmeron, G. A. Somorjai, *J. Am. Chem. Soc.* **2010**, *132*, 8697.
[29] F. Tao, M. E. Grass, Y. Zhang, D. R. Butcher, J. R. Renzas, Z. Liu, J. Y. Chung, B. S. Mun, M. Salmeron, G. A. Somorjai, *Science* **2008**, *322*, 932.
[30] S. Alayoglu, F. Tao, V. Altoe, C. Specht, Z. Zhu, F. Aksoy, D. R. Butcher, R. J. Renzas, Z. Liu, G. A. Somorjai, *Catal. Lett.* **2011**, *141*, 633.
[31] A. M. Venezia, L. F. Liotta, G. Pantaleo, V. La Parola, G. Deganello, A. Beck, Z. Koppány, K. Frey, D. Horváth, L. Guczi, *Appl. Catal. A* **2003**, *251*, 359.
[32] H. Bluhm, M. Hävecker, A. Knop-Gericke, E. Kleimenov, R. Schlögl, D. Teschner, V. I. Bukhtiyarov, D. F. Ogletree, M. Salmeron, *J. Phys. Chem. B* **2004**, *108*, 14340.
[33] T. Shimada, B. S. Mun, I. F. Nakai, A. Banno, H. Abe, Y. Iwasawa, T. Ohta, H. Kondoh, *J. Phys. Chem. C* **2010**, *114*, 17030.
[34] J. Stöhr, *NEXAFS*, *Vol. 25*, Springer, Heidelberg, **1992**.
[35] B. K. Teo, *EXAFS: basic principles and data analysis*, Springer, Heidelberg, **1986**.
[36] D. P. Woodruff, T. A. Delchar, *Modern techniques of surface science*, 2nd ed., Cambridge University Press, Cambridge, **1994**.
[37] M. O. Krause, *J. Phys. Chem. Ref. Data* **1979**, *8*, 307.
[38] W. A. Dench, M. P. Seah, *Practical surface analysis by Auger and X-ray photoelectron spectroscopy*, Wiley, New York, **1993**.
[39] F. Zheng, S. Alayoglu, J. Guo, V. Pushkarev, Y. Li, P. Glans, J. Chen, G. Somorjai, *Nano Lett.* **2011**, *11*, 847.
[40] T. Herranz, X. Deng, A. Cabot, J. Guo, M. Salmeron, *J. Phys. Chem. B* **2009**, *113*, 10721.
[41] A. Knop-Gericke, M. Hävecker, T. Schedel-Niedrig, R. Schlögl, *Top. Catal.* **2000**, *10*, 187.
[42] S. Zafeiratos, T. Dintzer, D. Teschner, R. Blume, M. Hävecker, A. Knop-Gericke, R. Schlögl, *J. Catal.* **2010**, *269*, 309.
[43] M. Bron, D. Teschner, A. Knop-Gericke, B. Steinhauer, A. Scheybal, M. Hävecker, D. Wang, R. Födisch, D. Hönicke, A. Wootsch, R. Schlögl, P. Claus, *J. Catal.* **2005**, *234*, 37.
[44] J. Stöhr, D. A. Outka, *Phys. Rev. B* **1987**, *36*, 7891.
[45] J.-D. Grunwaldt, S. Hannemann, C. G. Schroer, A. Baiker, *J. Phys. Chem. B* **2006**, *110*, 8674.
[46] J. A. van Bokhoven, C. Louis, J. T. Miller, M. Tromp, O. V. Safonova, P. Glatzel, *Angew. Chem.* **2006**, *118*, 4767; *Angew. Chem. Int. Ed.* **2006**, *45*, 4651.
[47] J.-D. Grunwaldt, B. S. Clausen, *Top. Catal.* **2002**, *18*, 37.
[48] M. A. Newton, A. J. Dent, S. Diaz-Moreno, S. G. Fiddy, J. Evans, *Angew. Chem.* **2002**, *114*, 2699; *Angew. Chem. Int. Ed.* **2002**, *41*, 2587.
[49] M. Rønning, N. E. Tsakoumis, A. Voronov, R. E. Johnsen, P. Norby, W. van Beek, Ø. Borg, E. Rytter, A. Holmen, *Catal. Today* **2010**, *155*, 289.
[50] C. Keresszegi, J. D. Grunwaldt, T. Mallat, A. Baiker, *J. Catal.* **2004**, *222*, 268.
[51] J.-D. Grunwaldt, M. Caravati, A. Baiker, *J. Phys. Chem. B* **2006**, *110*, 9916.
[52] G. D. Moggridge, T. Rayment, R. M. Ormerod, M. A. Morris, R. M. Lambert, *Nature* **1992**, *358*, 658.
[53] G. D. Moggridge, S. L. M. Schroeder, R. M. Lambert, T. Rayment, *Nucl. Instrum. Methods Phys. Res. Sect. B* **1995**, *97*, 28.
[54] P. J. Ellis, I. J. S. Fairlamb, S. F. J. Hackett, K. Wilson, A. F. Lee, *Angew. Chem.* **2010**, *122*, 1864; *Angew. Chem. Int. Ed.* **2010**, *49*, 1820.
[55] A. F. Lee, P. J. Ellis, I. J. S. Fairlamb, K. Wilson, *Dalton Trans.* **2010**, *39*, 10473.
[56] J. Evans, A. Puig-Molina, M. Tromp, *MRS Bull.* **2007**, *32*, 1038.
[57] C. A. Witham, W. Y. Huang, C. K. Tsung, J. N. Kuhn, G. A. Somorjai, F. D. Toste, *Nat. Chem.* **2010**, *2*, 36.
[58] M. C. Saint-Lager, A. Bailly, P. Dolle, R. Baudoing-Savois, P. Taunier, S. Garaudee, S. Cuccaro, S. Douillet, O. Geaymond, G. Perroux, O. Tissot, J. S. Micha, O. Ulrich, F. Rieutord, *Rev.Sci. Instrum.* **2007**, *78*, 083902.
[59] F. Gao, Y. Wang, D. W. Goodman, *J. Phys. Chem. C* **2009**, *113*, 14993.
[60] M. B. Pomfret, J. C. Owrutsky, R. A. Walker, *J. Phys. Chem. B* **2006**, *110*, 17305.

[61] T. Blasco, *Chem. Soc. Rev.* **2010**, *39*, 4685.
[62] E. D. Boyes, P. L. Gai, *Ultramicroscopy* **1997**, *67*, 219.
[63] J. F. Creemer, S. Helveg, G. H. Hoveling, S. Ullmann, A. M. Molenbroek, P. M. Sarro, H. W. Zandbergen, *Ultramicroscopy* **2008**, *108*, 993.
[64] M. Gajdardziska-Josifovska, R. Sharma, *Microsc. Microanal.* **2005**, *11*, 524.
[65] P. A. Crozier, R. Wang, R. Sharma, *Ultramicroscopy* **2008**, *108*, 1432.
[66] M. Cabié, S. Giorgio, C. R. Henry, M. Rosa Axet, K. Philippot, B. Chaudret, *J. Phys. Chem. C* **2011**, *114*, 2160.
[67] P. L. Gai, *Microsc. Microanal.* **2002**, *8*, 21.

